

# Beyond universality in repulsive SU(N) Fermi gases

Jordi Pera,<sup>1</sup> Joaquim Casulleras,<sup>1</sup> and Jordi Boronat<sup>1</sup>

*Departament de Física, Campus Nord B4-B5, Universitat Politècnica de Catalunya, E-08034 Barcelona, Spain*

(Dated: 15 June 2022)

Itinerant ferromagnetism in dilute Fermi gases is predicted to be at values of the gas parameter where second-order perturbation theory is not accurate enough. We have revisited perturbation theory up to third order for SU(N) fermions and found its generalization in terms of both the gas parameter and spin polarization. At difference with recent derivations of the same type at second-order, we have not been able to end up with a fully analytical result. Instead, we worked out analytically some of the terms and integrated numerically the rest. Our results agree satisfactorily with quantum Monte Carlo results for  $s = 1/2$  and hard-sphere interactions. For any value of the spin, we observe a discontinuous ferromagnetic transition but for  $s = 1/2$  the gap in the polarization at the transition is very small resembling more a quasi-continuous transition.

## I. INTRODUCTION

Trapped cold Fermi gases offer in principle an ideal platform to study itinerant ferromagnetism that, in real materials, has proven to be extremely elusive<sup>1,2</sup>. This transition must happen in the repulsive branch, which is metastable with respect to the formation of spin-up–spin-down dimers<sup>3</sup>. Recently, it has been reported that the ferromagnetic state is effectively observed in a Fermi <sup>7</sup>Li gas around a gas parameter  $x = k_F a_0 \simeq 1$ , with  $k_F$  the Fermi momentum and  $a_0$  the  $s$ -wave scattering length<sup>4</sup>. From a theoretical side, this transition has been extensively studied, mainly using quantum Monte Carlo methods<sup>5–12</sup>. These numerical estimations agree to localize the ferromagnetic transition around  $x \simeq 1$ . On the other hand, there is a growing interest in the theoretical description of Fermi gases with spins larger than  $1/2$ . In fact, dilute Fermi gases of Ytterbium<sup>13</sup>, with spin  $5/2$ , and Strontium<sup>14</sup>, with spin  $9/2$ , have been recently produced in experiments.

Another theoretical approach to study dilute Fermi gases relies on the use of perturbation theory. At first order, the famous Stoner model<sup>15</sup> predicts a continuous phase transition for  $s = 1/2$  and a first-order one for  $s > 1/2$ . As the Stoner model (Hartree-Fock approximation) is not accurate enough when the gas parameter grows, a second-order theory was developed long time ago<sup>16–19</sup>. Recently, this perturbative correction for SU(N) gases has been derived in a fully analytical form in terms of both polarization and gas parameter<sup>20</sup>. Previous results by Kanno<sup>21</sup> were limited to the hard-sphere potential and  $s = 1/2$ . At second order, one observes that the ferromagnetic transition for  $s = 1/2$  turns to be discontinuous breaking the asymmetry produced by the Stoner model.

Second-order perturbation energies improve substantially the Stoner model but still are not accurate enough to study Fermi gases close to the expected critical densities. Older results at third-order of perturbation theory are reported in Ref. [22]. However, to fully characterize the magnetic behavior of the Fermi gases it is fundamental to know the dependency of the energy on the gas parameter but also on the spin polarization<sup>23,24</sup>. In the present work, we derive the energy as a function of both parameters. At difference with second

order, we have not been able to end up with a completely fully analytical expression. Our results contain analytic contributions and also some numerical estimations. It is worth noticing that, going beyond second-order, breaks the universality of the expression, i.e., the dependence of the energy solely in terms of the  $s$ -wave scattering length. As we will see, two new scattering parameters enter into the description: the  $s$ -wave effective range and the  $p$ -wave scattering length.

For  $s = 1/2$ , we compare our predictions with diffusion Monte Carlo (DMC) results<sup>6</sup>. We obtain a nice agreement for hard-sphere fermions up to  $k_F a_0 \simeq 1$  where the ferromagnetic transition holds. Otherwise, we observe some systematic differences between our results and the DMC energies obtained for variable polarizations. Third-order perturbation theory does not change the order of the phase transition with respect to second order. However, for  $s = 1/2$  we observe that the discontinuity in the polarization at the transition is quite small turning it into a quasi-continuous one.

## II. METHODOLOGY

We study a repulsive Fermi gas at zero temperature with spin  $S$  and spin degeneracy  $\nu = 2S + 1$ . We have used perturbation theory and the final result is a combination of analytical results and numerical estimations. As we want to obtain the energy up to third order in the gas parameter, we will have particles with different  $z$ -spin component whose interactions will depend, not only on the  $s$ -wave scattering length, but also on the  $s$ -wave effective range and the  $p$ -wave scattering length. We will discuss the corresponding terms and calculate them. Each term implies the calculation of involved integrals. The first and second order terms have already been calculated in Ref. [20]. The terms coming from the  $s$ -wave effective range and the  $p$ -wave scattering length can be obtained analytically. However, the other contributions to the third order require a combination of analytical derivation and numerical integration.

The number of particles in each spin channel is  $N_\lambda = C_\lambda N/\nu$ , with  $N$  the total number of particles and  $C_\lambda$  being

the fraction of  $\lambda$  particles (normalized to be one if the system is unpolarized,  $N_\lambda = N/v$ ,  $\forall \lambda$ ). The Fermi momentum of each species is  $k_{F,\lambda} = k_F C_\lambda^{1/3}$ . The kinetic energy is readily obtained,

$$\frac{T}{N} = \frac{3}{5} \varepsilon_F \frac{1}{v} \sum_\lambda C_\lambda^{5/3}, \quad (1)$$

with  $\varepsilon_F$  the Fermi energy. The potential energy is the hard part, and to get it we applied perturbation theory. The formalism that we will work on is based on a Bishop report [22]. In essence, what is done is to calculate each Feynman diagram that contributes to each order of the expansion, and then to substitute the interaction by the K-matrix, which depends on the low-energy scattering parameters of the potential  $V(r)$ . We have generalized this procedure considering that all the Fermi species can have any occupation. The potential energy can be obtained by knowing the K-matrix through the expression,

$$V = \frac{\hbar^2 \Omega}{2m} \sum_{\lambda_1, \lambda_2} \int \frac{d\mathbf{l}}{(2\pi)^3} n_l \int \frac{d\mathbf{k}}{(2\pi)^3} n_k \times \{K(\mathbf{k}, \mathbf{l}; \mathbf{k}, \mathbf{l}) - \delta_{\lambda_1, \lambda_2} K(\mathbf{k}, \mathbf{l}; \mathbf{l}, \mathbf{k})\}, \quad (2)$$

with  $\Omega$  the volume, and  $n_l$  and  $n_k$  the momentum distributions of the free Fermi gas. Therefore, we have to integrate over two particles that are interacting between themselves through the K-matrix, which brings information on the potential. The K-matrix up to third order is<sup>22,25</sup>

$$K(\mathbf{r}, \mathbf{R}; \mathbf{r}', \mathbf{R}') = 4\pi a_0 + (4\pi a_0)^2 I(r, R) + (4\pi a_0)^3 I^2(r, R) + 4\pi \mathbf{r}^2 \frac{r_0}{2} a_0^2 + 4\pi a_1^3 \mathbf{r} \cdot \mathbf{r}' + O(a^4) \quad (3)$$

In Eq. (3),  $\mathbf{r} = (\mathbf{k} - \mathbf{l})/2$  and  $\mathbf{R} = \mathbf{R}' = \mathbf{k} + \mathbf{l}$  are the relative momentum and center of mass momentum, respectively.

---


$$F(y) = \frac{1}{4} (15y^2 - 19y + 52 - 19y^{-1} + 15y^{-2}) + \frac{7}{8} y^{-2} (y-1)^4 (y+3+y^{-1}) \ln \left| \frac{1-y}{1+y} \right| - \frac{2y^4}{1+y} \ln \left| 1 + \frac{1}{y} \right| - \frac{2y^{-4}}{1+y^{-1}} \ln \left| 1+y \right| \quad (9)$$

and  $y \equiv (C_{\lambda_1}/C_{\lambda_2})^{1/3}$ . It is worth noticing that this term agrees with the Kanno result obtained for  $s = 1/2$  fermions<sup>21</sup>.

In the following subsections, we will solve the new terms, that is the ones contributing to the third order in the gas parameter.

### A. S-wave effective range term

Beyond second-order, one needs to introduce additional scattering parameters other than the s-wave scattering length

For  $K(\mathbf{k}, \mathbf{l}; \mathbf{k}, \mathbf{l})$ ,  $\mathbf{r}' = \mathbf{r}$ , whereas for  $K(\mathbf{k}, \mathbf{l}; \mathbf{l}, \mathbf{k})$ ,  $\mathbf{r}' = -\mathbf{r}$ . The function  $I(r, R)$  is defined as

$$I(r, R) = \frac{1}{(2\pi)^3} \times \int 2d\mathbf{q}d\mathbf{q}' \frac{1 - (1-n_q)(1-n_{q'})}{q^2 + q'^2 - k^2 - l^2} \delta(\mathbf{q} + \mathbf{q}' - \mathbf{k} - \mathbf{l}). \quad (4)$$

Considering only the first term in the expansion of the K-matrix (3), one gets for the potential energy (2) the well-know Hartree-Fock energy<sup>15</sup>,

$$\left(\frac{V}{N}\right)_1 = \frac{2\varepsilon_F}{3\pi} \left[ \frac{1}{v} \sum_{\lambda_1, \lambda_2} C_{\lambda_1} C_{\lambda_2} (1 - \delta_{\lambda_1, \lambda_2}) \right] x, \quad (5)$$

with  $x \equiv k_F a_0$  the gas parameter of the Fermi gas.

The second order term in the gas parameter  $x$  is due to the second term of the K-matrix. This second order term reads

$$\left(\frac{V}{N}\right)_2 = \frac{\varepsilon_F}{k_F^7} \left[ \frac{1}{v} \sum_{\lambda_1, \lambda_2} I_2(k_{F,\lambda_1}, k_{F,\lambda_2}) (1 - \delta_{\lambda_1, \lambda_2}) \right] x^2, \quad (6)$$

with

$$I_2(C_{\lambda_1}, C_{\lambda_2}) = \frac{3}{16\pi^5} \int d\mathbf{l} n_l \int d\mathbf{k} n_k \int 2d\mathbf{q}d\mathbf{q}' \times \frac{1 - (1-n_q)(1-n_{q'})}{q^2 + q'^2 - k^2 - l^2} \delta(\mathbf{q} + \mathbf{q}' - \mathbf{k} - \mathbf{l}). \quad (7)$$

The term  $I_2(C_{\lambda_1}, C_{\lambda_2})$  was already obtained in Ref. [20]. The solution is

$$I_2(C_{\lambda_1}, C_{\lambda_2}) = \frac{4k_F^7}{35\pi^2} C_{\lambda_1} C_{\lambda_2} \frac{C_{\lambda_1}^{1/3} + C_{\lambda_2}^{1/3}}{2} F(y), \quad (8)$$

with

---

and thus the expression is no longer universal. The effective range term in the K-matrix is:  $K = 4\pi \mathbf{r}^2 \frac{1}{2} r_0 a_0^2$ . First of all, we express  $\mathbf{r}^2$  in terms of  $\mathbf{k}$  and  $\mathbf{l}$ ,

$$\mathbf{r}^2 = \frac{1}{4} (\mathbf{k} - \mathbf{l})^2 = \frac{1}{4} (k^2 + l^2 - 2kl \cos \theta) \quad (10)$$

Then, we substitute the value of  $K$  in Eq. (2) and integrate. The term containing  $\cos \theta$  gives zero after doing the angular

integration,

$$\begin{aligned}
E &= \frac{\hbar^2 V}{2m} \sum_{\lambda_1, \lambda_2} \int \frac{d\mathbf{l}}{(2\pi)^3} n_l \int \frac{d\mathbf{k}}{(2\pi)^3} n_k \\
&\quad \times \frac{4\pi r_0 a_0^2}{8} (k^2 + l^2 - 2kl \cos \theta) (1 - \delta_{\lambda_1, \lambda_2}) \\
&= \frac{\hbar^2 V}{2m} \sum_{\lambda_1, \lambda_2} \frac{1}{8\pi^3} \left( \frac{k_{F, \lambda_1}^3}{3} \frac{k_{F, \lambda_2}^5}{5} + \frac{k_{F, \lambda_1}^5}{5} \frac{k_{F, \lambda_2}^3}{3} \right) r_0 a_0^2 (1 - \delta_{\lambda_1, \lambda_2})
\end{aligned} \tag{11}$$

The energy per particle as a function of  $C_\lambda$  is

$$\begin{aligned}
\frac{E}{N} &= \varepsilon_F \frac{1}{v} \sum_{\lambda_1, \lambda_2} \frac{1}{10\pi} \\
&\times C_{\lambda_1} C_{\lambda_2} \left( \frac{C_{\lambda_1}^{2/3} + C_{\lambda_2}^{2/3}}{2} \right) (k_F r_0) (k_F a_0)^2 (1 - \delta_{\lambda_1, \lambda_2}).
\end{aligned} \tag{12}$$

## B. P-wave term

As before, we first show the corresponding term in the  $K$ -matrix. One needs to be careful because this term depends also on  $\mathbf{r}'$ , at difference with the effective range term. The two  $K$ -matrix terms that we need differ by a minus sign:  $K(\mathbf{k}, \mathbf{l}; \mathbf{k}, \mathbf{l}) = 4\pi a_1^3 \mathbf{r}^2$ ,  $K(\mathbf{k}, \mathbf{l}; \mathbf{l}, \mathbf{k}) = -4\pi a_1^3 \mathbf{r}^2$ . This negative sign causes the term proportional to the Kronecker delta to change its sign. And this change of sign introduces interaction between particles of the same spin. Perhaps, this fact is not evident, but, once we have integrated and rearranged terms, it will be. The integral to do, apart from the negative sign, is formally the same as the one calculated for the effective range. Hence, the energy per particle is:

$$\frac{E}{N} = \varepsilon_F \frac{1}{v} \sum_{\lambda_1, \lambda_2} \frac{1}{5\pi} C_{\lambda_1} C_{\lambda_2} \left( \frac{C_{\lambda_1}^{2/3} + C_{\lambda_2}^{2/3}}{2} \right) (k_F a_1)^3 (1 + \delta_{\lambda_1, \lambda_2}). \tag{13}$$

If we look to the term  $(1 + \delta_{\lambda_1, \lambda_2})$ , we see that it is equivalent to  $2\delta_{\lambda_1, \lambda_2} + (1 - \delta_{\lambda_1, \lambda_2})$ , so we have interaction between pairs of different spin, as in all previous terms; they are all proportional to  $(1 - \delta_{\lambda_1, \lambda_2})$ . But now we also have a term  $2\delta_{\lambda_1, \lambda_2}$ , which will give rise to an extra interaction term between particles of same spin. For this new contribution, called  $P$ -wave interaction between particles of same spin, we obtain

$$\begin{aligned}
\frac{E}{N} &= \varepsilon_F \frac{1}{v} \sum_{\lambda_1, \lambda_2} \frac{1}{5\pi} C_{\lambda_1} C_{\lambda_2} \left( \frac{C_{\lambda_1}^{2/3} + C_{\lambda_2}^{2/3}}{2} \right) (k_F a_1)^3 (2\delta_{\lambda_1, \lambda_2}) \\
&= \frac{3}{5} \varepsilon_F \frac{1}{v} \sum_{\lambda} \frac{2}{3\pi} C_\lambda^{8/3} (k_F a_1)^3.
\end{aligned} \tag{14}$$

If we split Eq. (13) in two parts, one part containing the interaction between particles of different spin and another one

with this new contribution, one gets

$$\begin{aligned}
\frac{E}{N} &= \frac{3}{5} \varepsilon_F \left[ \frac{1}{v} \sum_{\lambda} \frac{2}{3\pi} C_\lambda^{8/3} (k_F a_1)^3 \right. \\
&\quad \left. + \frac{5}{3v} \sum_{\lambda_1, \lambda_2} \frac{1}{5\pi} C_{\lambda_1} C_{\lambda_2} \left( \frac{C_{\lambda_1}^{2/3} + C_{\lambda_2}^{2/3}}{2} \right) (k_F a_1)^3 (1 - \delta_{\lambda_1, \lambda_2}) \right].
\end{aligned} \tag{15}$$

However, our work is intended for the study of highly degenerate Fermi gases under the assumption that  $P$ -wave interaction between particles of same spin is negligible. Therefore, although we have been able to obtain this term, this term will not be considered in the Results section.

## C. 3rd order terms

Due to their mathematical complexity, we have not been able to calculate the third order terms in a closed analytical form. We were forced to use numerical integration in order to calculate these terms. We have three contributions at third order, we show them in Eqs. (16), (17) and (18). The objects we have calculated numerically are  $E_3$ ,  $E_4$  and  $E_5$ . The three functions are normalized expressions, so we can compare the results for different spins. The integral  $E_3$  is

$$\begin{aligned}
E_3 &= \frac{1}{v(v-1)k_F^8} \sum_{\lambda_1, \lambda_2} I_3(k_{F, \lambda_1}, k_{F, \lambda_2}) (1 - \delta_{\lambda_1, \lambda_2}) \\
&\quad \text{where } I_3(k_{F, \lambda_1}, k_{F, \lambda_2}) = \frac{3}{32\pi^7} \int d\mathbf{l} n_l \int d\mathbf{k} n_k \\
&\quad \times \left[ \int 2d\mathbf{q} d\mathbf{q}' \frac{1 - (1 - n_q)(1 - n_{q'})}{q^2 + q'^2 - k^2 - l^2} \delta(\mathbf{q} + \mathbf{q}' - \mathbf{k} - \mathbf{l}) \right]^2.
\end{aligned} \tag{16}$$

We have another pair-like term ( $E_4$ ), given by

$$\begin{aligned}
E_4 &= \frac{1}{v(v-1)k_F^8} \sum_{\lambda_1, \lambda_2} I_4(k_{F, \lambda_1}, k_{F, \lambda_2}) (1 - \delta_{\lambda_1, \lambda_2}) \\
&\quad \text{with } I_4(k_{F, \lambda_1}, k_{F, \lambda_2}) = \frac{3}{32\pi^7} \int d\mathbf{m} (1 - n_m) \int d\mathbf{m}' (1 - n_{m'}) \\
&\quad \times \left[ \int 2d\mathbf{p} d\mathbf{p}' \frac{n_p n_{p'}}{p^2 + p'^2 - m^2 - m'^2} \delta(\mathbf{p} + \mathbf{p}' - \mathbf{m} - \mathbf{m}') \right]^2.
\end{aligned} \tag{17}$$

Finally, there is one last term containing the interaction between three particles. Its expression is even more involved

than the previous ones,

$$E_5 = \frac{1}{v(v-1)k_F^8} \sum_{\lambda_1, \lambda_2} I_5(k_{F, \lambda_1}, k_{F, \lambda_2})(1 - \delta_{\lambda_1, \lambda_2})$$

$$\text{where } I_5(k_{F, \lambda_1}, k_{F, \lambda_2}) = \frac{3}{32\pi^7(v-3)} \left[ 2 \sum_{\lambda_3 \neq (\lambda_1, \lambda_2)} \bar{F}_{\lambda_3, \lambda_1, \lambda_2} - \bar{F}_{\lambda_1, \lambda_1, \lambda_2} - \bar{F}_{\lambda_2, \lambda_1, \lambda_2} \right]$$

$$\begin{aligned} & \text{with } \bar{F}[k_{F, \lambda_3}, k_{F, \lambda_1}, k_{F, \lambda_2}] = \int d\mathbf{m}(1-n_m) \int d\mathbf{p} n_p \\ & \times \left[ \int 2d\mathbf{m}' d\mathbf{p}' \frac{(1-n_{m'})n_{p'}}{p^2 + p'^2 - m^2 - m'^2} \delta(\mathbf{p} + \mathbf{p}' - \mathbf{m} - \mathbf{m}') \right] \\ & \times \left[ \int 2d\mathbf{m}'' d\mathbf{p}'' \frac{(1-n_{m''})n_{p''}}{p^2 + p''^2 - m^2 - m''^2} \delta(\mathbf{p} + \mathbf{p}'' - \mathbf{m} - \mathbf{m}'') \right] \end{aligned} \quad (18)$$

These integrals have been computed for different values of the polarization. To help in the posterior numerical manipulation, we performed a polynomial fitting to the obtained data. As the integrals of the potential become zero when the polarization is  $\pm 1$ , the polynomial can be factorized as  $(1-P)(1+P)H(P)$ . Where  $H(P)$  is another polynomial. The function used for the fitting is

$$F(P) = A(1-P^2)(1 + b_1P^2 + b_2P^4 + b_3P^6 + b_4P^8). \quad (19)$$

The parameter  $A$  is not a parameter to fit, this is the value of the integrals for zero polarization. These values are already known because they have been obtained in other works that studied Fermi gases at zero polarization [17,16,18,19,26,27]. Even though, we have computed them again in order to check that the values are correct. We have used  $10^8$  points for a

Monte Carlo integration. The values obtained are reported in Table I and compare well with previous estimations [22].

Present work	Ref.[22]
$A_{E_3} = 0,06406 \pm 2 \cdot 10^{-5}$	$A_{E_3} = 0,06406$
$A_{E_4} = 0,011489 \pm 3 \cdot 10^{-6}$	$A_{E_4} = 0,01148 \pm 2 \cdot 10^{-5}$
$A_{E_5} = 0,05729 \pm 2 \cdot 10^{-5}$	$A_{E_5} = 0,05726 \pm 4 \cdot 10^{-5}$

TABLE I. Values of the parameter  $A$  for  $E_3$ ,  $E_4$  and  $E_5$  computed by us and Bishop<sup>22</sup>.

In order to compute the numerical integrals for spins higher than  $1/2$ , we have assumed that when the concentration of one species increases, all the rest diminish in the same manner. This is the configuration that minimizes the energy when  $N$  is constant. Under these conditions, the concentrations  $C_\lambda$  for a given polarization  $P$  are

$$C_+ = 1 + |P|(v-1) \quad (20)$$

$$C_{\lambda \neq +} = 1 - |P|, \quad (21)$$

with subindex  $+$  standing for the state with the larger population. This definition of polarization has been justified in Ref. [20]. The fitted parameters can be found in Appendices.

#### D. Final formula

Finally, we present all the terms calculated until this point in a single formula. In Eq. (22), there are, in the first line, the kinetic energy, the  $P$ -wave interaction between particles of equal spin (neglected in the results) and the two first orders of the perturbative expansion (universal expansion). Then, there are the terms corresponding to the  $S$ -wave effective range, the  $P$ -wave scattering length and the numerical terms ( $E_3$ ,  $E_4$  i  $E_5$ ) of third order,

$$\begin{aligned} \frac{E}{N} = & \frac{3}{5} \varepsilon_F \left[ \frac{1}{v} \sum_{\lambda} C_{\lambda}^{5/3} + \frac{1}{v} \sum_{\lambda} \frac{2}{3\pi} C_{\lambda}^{8/3} (k_F a_1)^3 + \frac{5}{3v} \sum_{\lambda_1, \lambda_2} \left\{ \frac{2}{3\pi} (k_F a_0) C_{\lambda_1} C_{\lambda_2} + \frac{4k_F^7}{35\pi^2} C_{\lambda_1} C_{\lambda_2} \frac{C_{\lambda_1}^{1/3} + C_{\lambda_2}^{1/3}}{2} F(y) (k_F a_0)^2 \right. \right. \\ & \left. \left. + \frac{1}{10\pi} C_{\lambda_1} C_{\lambda_2} \left( \frac{C_{\lambda_1}^{2/3} + C_{\lambda_2}^{2/3}}{2} \right) \left[ \frac{r_0}{a_0} + 2 \frac{a_1^3}{a_0^3} \right] (k_F a_0)^3 \right\} (1 - \delta_{\lambda_1, \lambda_2}) + \frac{5}{3} (v-1) (E_3 + E_4 + (v-3)E_5) (k_F a_0)^3 \right]. \end{aligned} \quad (22)$$

### III. RESULTS

In this section, we discuss the main features of  $SU(N)$  Fermi gases using the formalism derived in the precedent Section. Now we have two more scattering parameters than the case of an universal expansion (second order). This means that the specific potential model influences the derived results beyond the simple dependence on the  $s$ -wave scattering length. As we are considering a repulsive gas, we will work under the assumption of a hard-spheres potential ( $r_0 = 2a_0/3$ ,  $a_1 = a_0$ ) since this is somehow a more universal model. We

present the results for three different spins:  $s = 1/2$ ,  $s = 5/2$  (Ytterbium) and  $s = 9/2$  (Strontium).

Having at hand a perturbative prediction allows us to compare our results with available quantum Monte Carlo data. We compare our prediction with diffusion Monte Carlo data for spin  $1/2$  <sup>6</sup> in Fig. 1. As commented previously, we do not include  $p$ -wave scattering terms between particles of same  $z$ -spin component, as it is also done in the DMC simulations. Apart from the DMC points, we show four lines. The orange one correspond to the fully-polarized gas. The blue one to the non-polarized gas. The green line to the configuration of

minimum energy, that is: at each value of the density, we use the polarization that minimizes the energy. And lastly, there is a red line that corresponds to the second order energy (universal expansion) in order to compare with the third order expansion that we are using now. We can see how the second-order and the third-order expansions reproduce the same energy for values of  $k_F a_0 < 0.4$ . Beyond that, the difference intensifies with increasing density. Concerning the DMC points, although they are upper-bounds to the exact energy due to the sign problem, they fit pretty well the third-order curve.

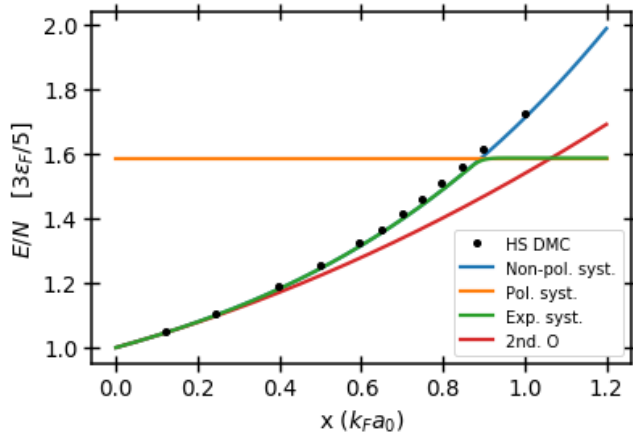


FIG. 1. Energy for  $s = 1/2$  as a function of the gas parameter. We plot two models: in green, the third-order model; in red, the second-order one. The points are DMC results<sup>6</sup>.

Another important feature that we can calculate thanks to having an accurate expression is the energy as a function of the polarization. In Fig. 2, we show our results for different gas parameters. One can see that, until a gas parameter of  $k_F a_0 = 0,85$ , the polarization that minimizes the energy is zero. However, at  $k_F a_0 = 0,9$ , the minimum of the energy moves to a higher polarization. Concerning the DMC points, we observe that there must be some systematic error because all the points near zero polarization have higher values than they should. Moreover, the error is not coming from our results, because around  $P = 0$  they coincide with this previous studied case.

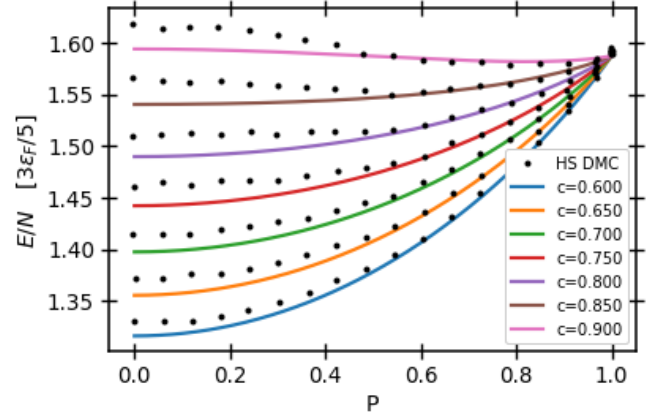


FIG. 2. Energy per particle as a function of the polarization for different values of the gas parameter ( $s = 1/2$ ). The points stand for DMC results<sup>6</sup>.

In Fig. (3), we show the energy as a function of the gas parameter for the three spin values about we are mainly interested ( $s = 1/2, 5/2$  and  $9/2$ ). For the case of hard-spheres, the third-order model predicts a first-order phase transition for the three spins. We also see that with increasing spin, the transition occurs at lower values of the gas parameter.

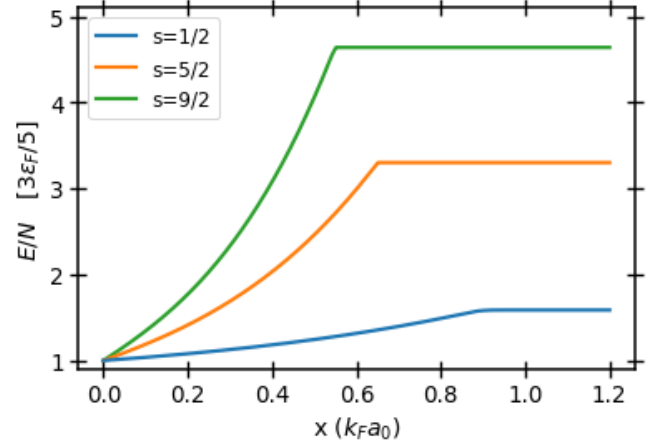


FIG. 3. Energy per particle as a function of the gas parameter for three spins  $s = 1/2, 5/2$  and  $9/2$ .

A more useful figure (Fig. 4) to observe a phase transition is to plot the order parameter (in this case the polarization) as a function of the gas parameter. Indeed, as we have said, the three cases goes from a non-polarized gas to a fully-polarized one. But there is a significant difference. For spin  $5/2$  and  $9/2$ , the transition is clearly discontinuous. However, for spin  $1/2$ , if it is not continuous, it is a quasi-continuous transition. This fact contrasts with the result reported in Ref.[] where the transition for spin  $1/2$  was discontinuous and had a polarization jump of 0.545.

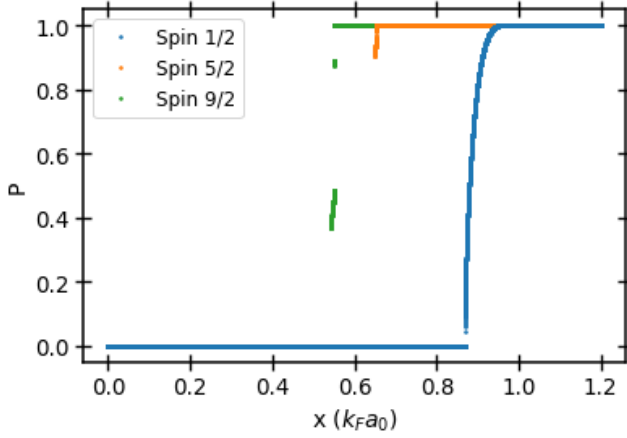


FIG. 4. Polarization as a function of the gas parameter for three spins  $s = 1/2, 5/2$  and  $9/2$ .

Important information on the system is contained in the magnetic susceptibility  $\chi$ ,

$$\frac{1}{\chi} = \frac{1}{n} \left( \frac{\partial^2 (E/N)}{\partial P^2} \right)_x. \quad (23)$$

In Fig. 5, we plot  $\chi$  for spin  $1/2$ ; in Fig. 6, we plot the other two spins. The reason of this split lies on the fact that the plot for spin  $1/2$  has much larger values than the other two cases. The behavior of the magnetic susceptibility for spin  $1/2$  agrees with what we have shown above when discussing the behavior of the polarization. The magnetic susceptibility has a strong peak around  $k_F a_0 = 0,85$  corresponding to a the quasi-continuous phase transition. The other two spins do not exhibit this high peak, therefore, we reassert the discontinuous nature of the phase transition.

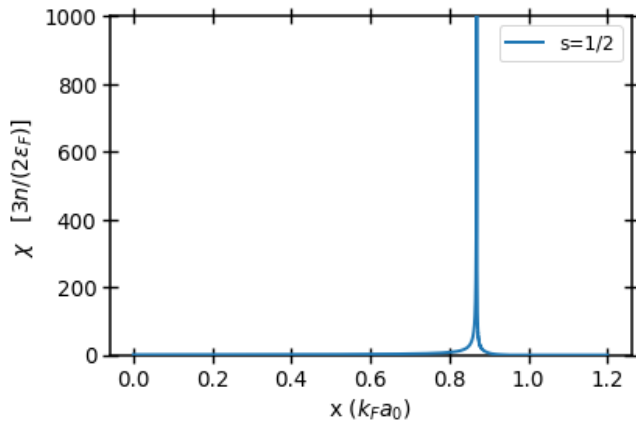


FIG. 5. Magnetic susceptibility as a function of the gas parameter for spin  $s = 1/2$ .

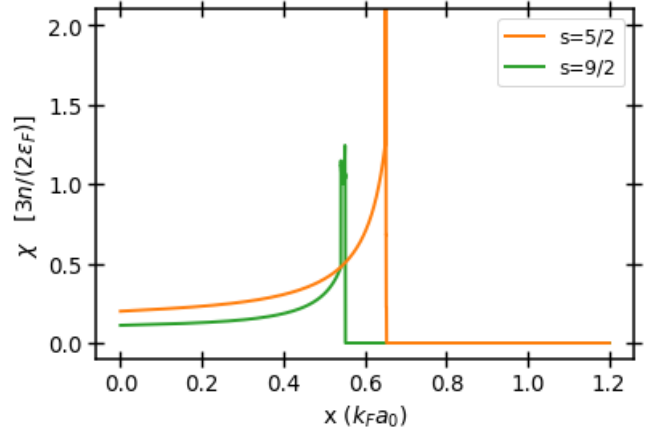


FIG. 6. Magnetic susceptibility as a function of the gas parameter for spins  $s = 5/2$  and  $9/2$ .

For the sake of completeness, we show the Tan's constant (Fig. 7). The Tan's constant,

$$C = \frac{4\pi m a_0^2 N}{\hbar^2 V} \frac{\partial (E/N)}{\partial a_0}, \quad (24)$$

is a very good identifier if one wants to find the density at which the transition occurs. It is so, because right before the transition, the Tan's constant is maximum. Looking to the Tan's constant for the three spins, we can see again that the transition happens at lower densities when the degeneracy increases.

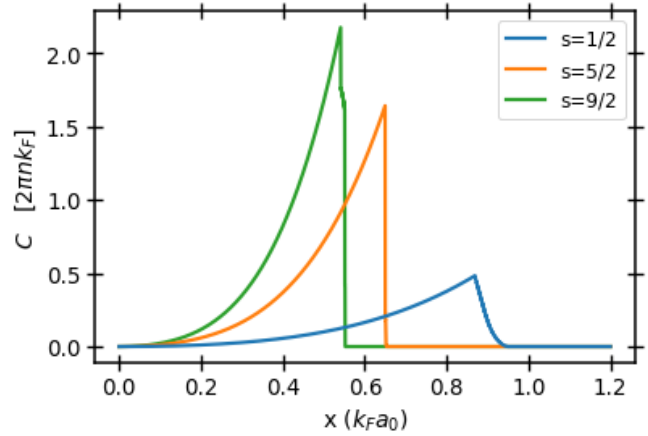


FIG. 7. Tan's constant as a function of the gas parameter for three spins,  $s = 1/2, 5/2$  and  $9/2$ .

As commented before, the ferromagnetic phase transition happens at lower densities if we increase the spin of the gas. In Fig. 8, we show the critical gas parameter as a function of the spin value, up to spin  $15/2$ . We point out that for spin  $15/2$ , the transition gas parameter is  $0.44$ , which is very low. For Ytterbium ( $s = 5/2$ ), the gas parameter is  $0.65$ , and for Strontium ( $s = 9/2$ ) is  $0.53$ .

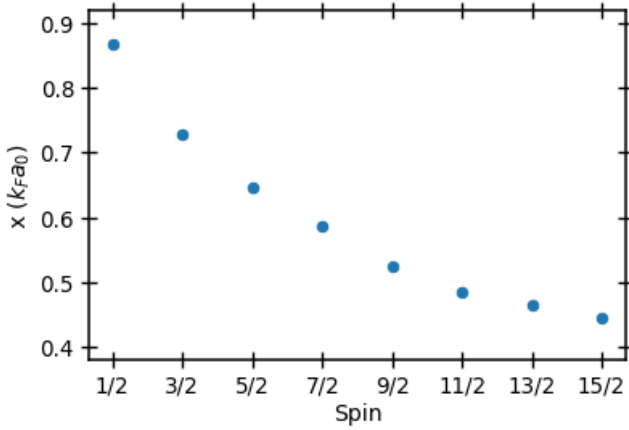


FIG. 8. Critical gas parameter as a function of the spin value.

#### IV. CONCLUSIONS

Summarizing, we obtained the expression of the energy of a repulsive  $SU(N)$  Fermi gas up to third-order in the gas parameter in terms of the spin-channel occupations. We have been able to extend up to third order our previous result in Ref.[20] where we obtained the universal expansion (second order). We included the S-wave effective range term, the P-wave scattering length term and more third-order terms that have been calculated numerically.

The third-order expression allows to reproduce and test numerical values obtained with diffusion Monte Carlo. Concerning itinerant ferromagnetism, as now there are three scattering parameters in game, the phase transition is not guaranteed. However, under certain potentials, the values for the scattering parameters up to third-order may allow itinerant ferromagnetism, this is the case, for example, of a hard-spheres potential, the one we have used for our results. For a hard-spheres potentials and using the third-order model, the gas of spin  $1/2$  exhibits a quasi-continuous magnetic phase transition (approaching the continuous phase transition of the Stoner model). For higher spins values, the transition is clearly first-order. Including the third-order term diminishes much more the value of the gas parameter at which the ferromagnetic transition occurs. For spin  $5/2$ , it occurs at  $k_F a_0 = 0.65$ ; and for spin  $9/2$ , at  $k_F a_0 = 0.53$ . This fact reinforces the idea that the observation of itinerant ferromagnetism could be favored by working with highly-degenerate gases as Yb [13] and Sr [14].

#### ACKNOWLEDGMENTS

We acknowledge financial support from MCIN/AEI/10.13039/501100011033 (Spain) grant No. PID2020-113565GB-C21 and from Secretaria d'Universitats i Recerca del Departament d'Empresa i Coneixement de la Generalitat de Catalunya, co-funded by the European

Union Regional Development Fund within the ERDF Operational Program of Catalunya (project QuantumCat, ref. 001-P-001644).

#### Appendix A: Tables with their associated plots

##### 1. Spin $1/2$

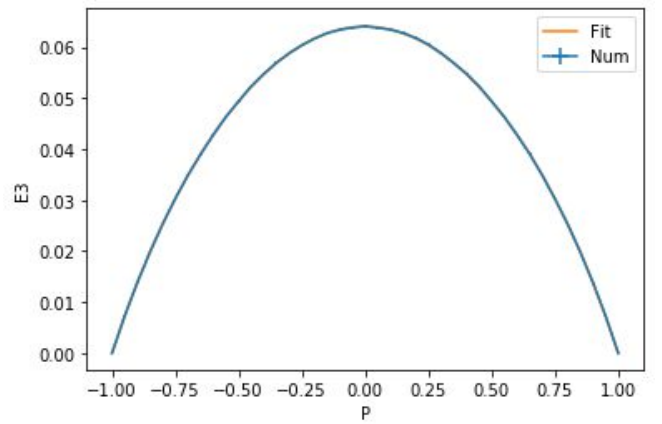


FIG. 9. Integral E3 as a function of the polarization for the case  $s = 1/2$ . The error-bars are smaller than the width of the line. The fitting is also represented but it is behind the blue line.

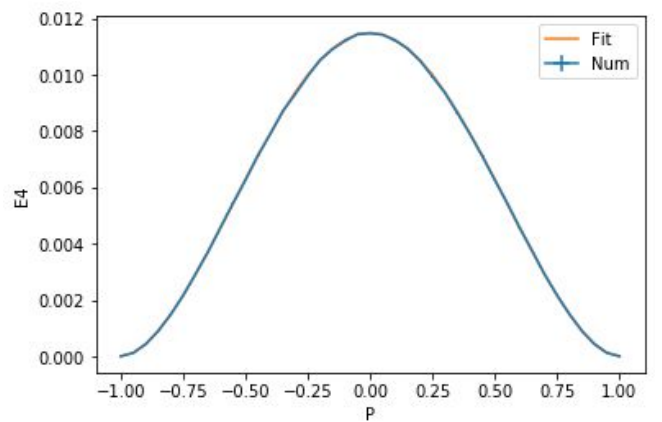


FIG. 10. Integral E4 as a function of the polarization for the case  $s = 1/2$ . The error-bars are smaller than the width of the line. The fitting is also represented but it is behind the blue line.

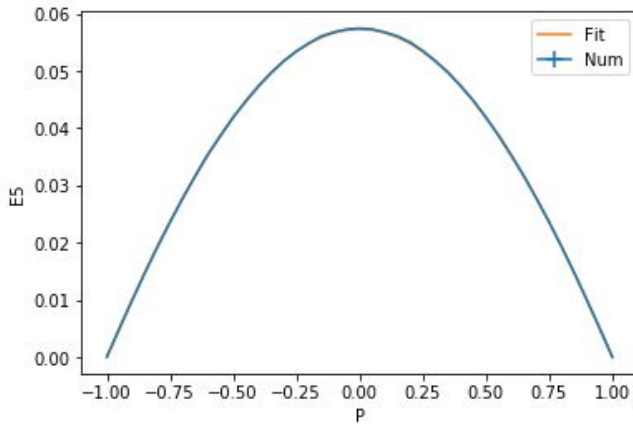


FIG. 11. Integral  $E_5$  as a function of the polarization for the case  $s = 1/2$ . The error-bars are represented, however they are smaller than the width of the line. The fitting is also represented but it is behind the blue line.

	$b_1$	$b_2$	$b_3$	$b_4$	$\chi^2_{red}$
$E_3$	$0.087 \pm 0.002$	$0.104 \pm 0.003$			0.21
$E_4$	$-1.182 \pm 0.006$	$0.445 \pm 0.017$	$-0.257 \pm 0.012$		1.82
$E_5$	$-0.097 \pm 0.002$	$-0.018 \pm 0.003$			2.05

TABLE II. Parameters of the fit with their uncertainties, and the reduced chi square associated with each fitting for the case  $s = 1/2$ . The blank spaces can be considered to be zero

## 2. Spin 3/2

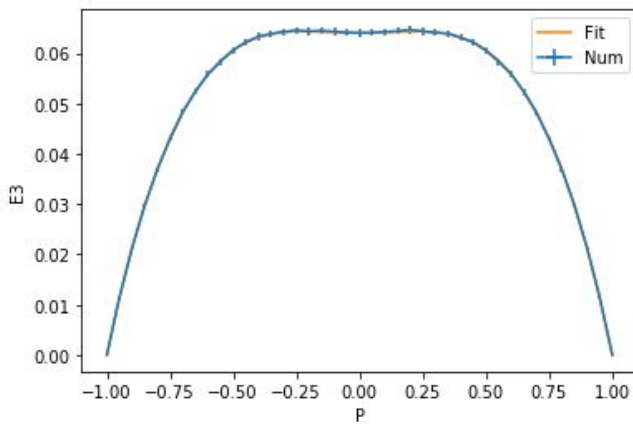


FIG. 12. Integral  $E_3$  as a function of the polarization for the case  $s = 3/2$ . The error-bars are smaller than the width of the line. The fitting is also represented but it is behind the blue line.

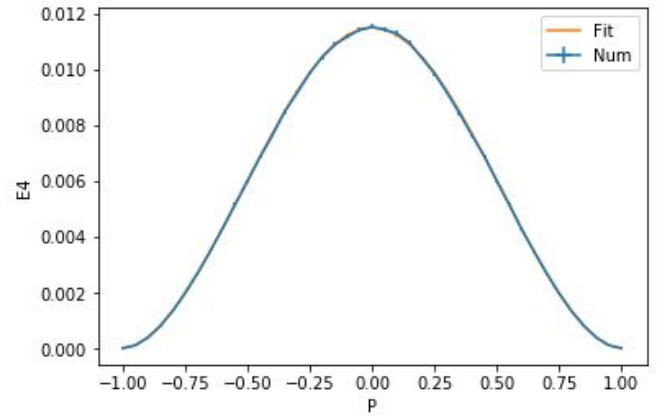


FIG. 13. Integral  $E_4$  as a function of the polarization for the case  $s = 3/2$ . The error-bars are smaller than the width of the line. The fitting is also represented but it is behind the blue line.

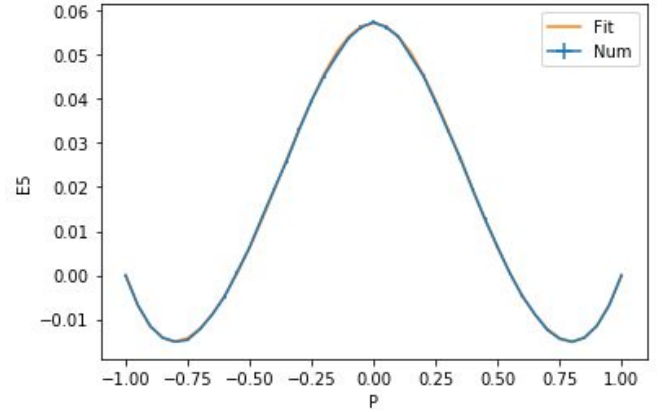


FIG. 14. Integral  $E_5$  as a function of the polarization for the case  $s = 3/2$ . The error-bars are smaller than the width of the line. The fitting is also represented but it is behind the blue line.

	$b_1$	$b_2$	$b_3$	$b_4$	$\chi^2_{red}$
$E_3$	$1.178 \pm 0.008$	$-0.61 \pm 0.03$	$0.37 \pm 0.02$		0.03
$E_4$	$-1.368 \pm 0.007$	$0.69 \pm 0.02$	$-0.316 \pm 0.014$		0.28
$E_5$	$-4.50 \pm 0.03$	$5.72 \pm 0.2$	$-6.3 \pm 0.4$	$2.8 \pm 0.2$	0.68

TABLE III. Parameters of the fit with their uncertainties, and the reduced chi square associated with each fitting for the case  $s = 3/2$ . The blank spaces can be considered to be zero



### 3. Spin 5/2

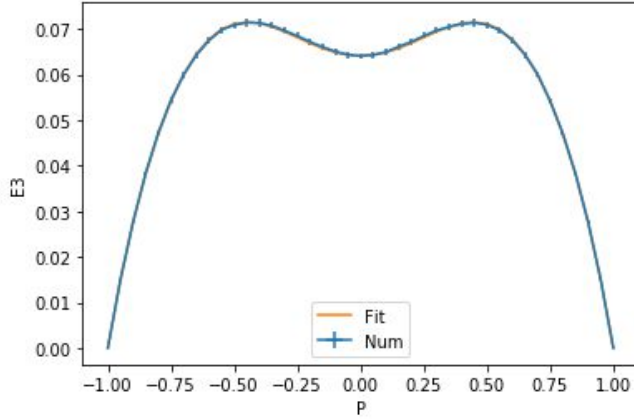


FIG. 15. Integral E3 as a function of the polarization for the case  $s = 5/2$ . The error-bars are smaller than the width of the line. The fitting is also represented but it is behind the blue line.

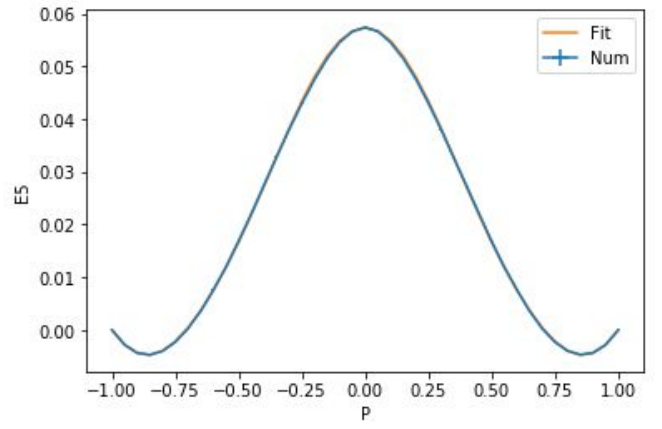


FIG. 17. Integral E5 as a function of the polarization for the case  $s = 5/2$ . The error-bars are smaller than the width of the line. The fitting is also represented but it is behind the blue line.

	$b_1$	$b_2$	$b_3$	$b_4$	$\chi^2_{red}$
$E_3$	$2.236 \pm 0.013$	$-1.48 \pm 0.05$	$0.82 \pm 0.05$		0.07
$E_4$	$-1.503 \pm 0.010$	$0.884 \pm 0.03$	$-0.382 \pm 0.019$		0.49
$E_5$	$-3.35 \pm 0.03$	$4.76 \pm 0.18$	$-5.3 \pm 0.3$	$2.3 \pm 0.2$	2.18

TABLE IV. Parameters of the fit with their uncertainties, and the reduced chi square associated with each fitting for the case  $s = 5/2$ . The blank spaces can be considered to be zero

### 4. Spin 7/2

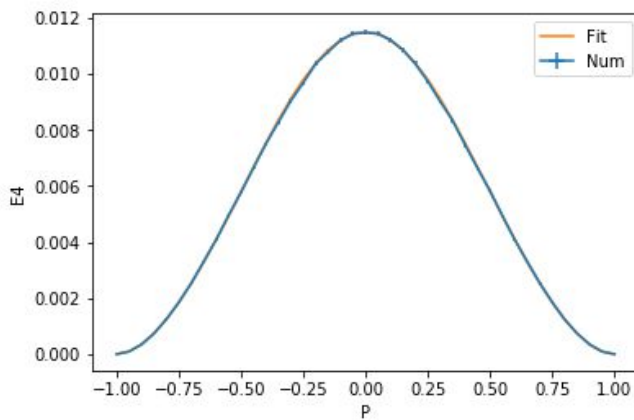


FIG. 16. Integral E4 as a function of the polarization for the case  $s = 5/2$ . The error-bars are smaller than the width of the line. The fitting is also represented but it is behind the blue line.

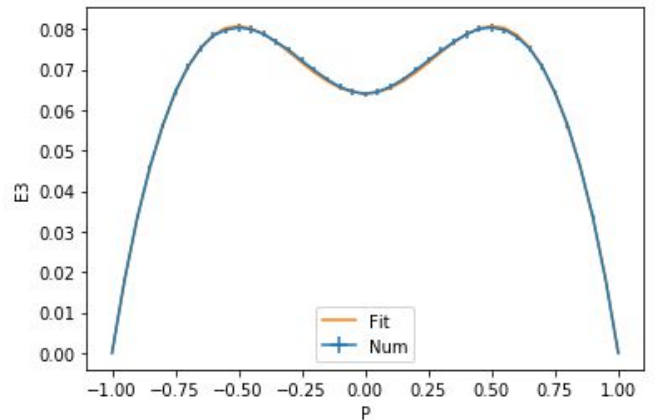


FIG. 18. Integral E3 as a function of the polarization for the case  $s = 7/2$ . The error-bars are smaller than the width of the line. The fitting is also represented but it is behind the blue line.

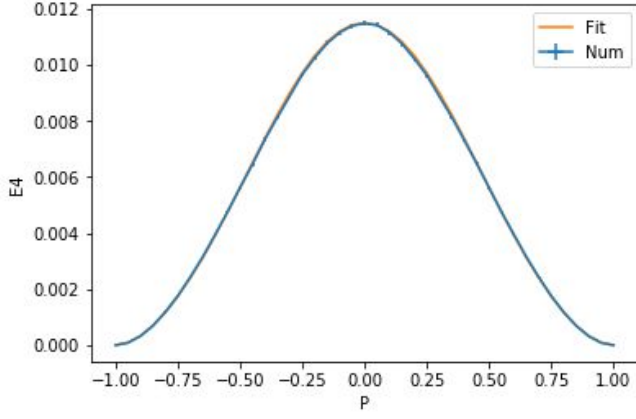


FIG. 19. Integral  $E_4$  as a function of the polarization for the case  $s = 7/2$ . The error-bars are smaller than the width of the line. The fitting is also represented but it is behind the blue line.

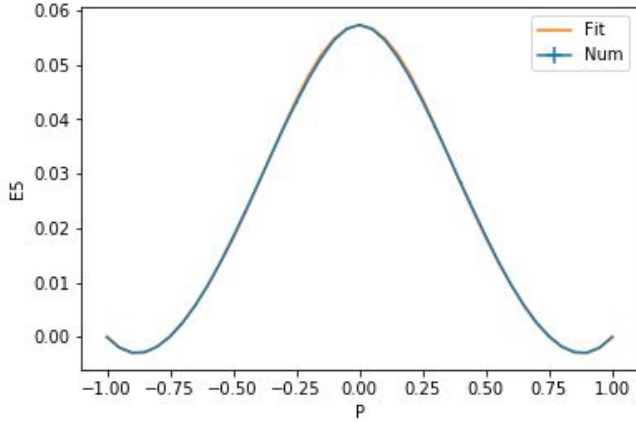


FIG. 20. Integral  $E_5$  as a function of the polarization for the case  $s = 7/2$ . The error-bars are smaller than the width of the line. The fitting is also represented but it is behind the blue line.

	$b_1$	$b_2$	$b_3$	$b_4$	$\chi_{red}^2$
$E_3$	$3.26 \pm 0.02$	$-2.46 \pm 0.09$	$1.35 \pm 0.08$		0.19
$E_4$	$-1.643 \pm 0.012$	$1.14 \pm 0.03$	$-0.50 \pm 0.02$		0.73
$E_5$	$-3.29 \pm 0.03$	$5.2 \pm 0.2$	$-5.9 \pm 0.4$	$2.6 \pm 0.2$	5.49

TABLE V. Parameters of the fit with their uncertainties, and the reduced chi square associated with each fitting for the case  $s = 7/2$ . The blank spaces can be considered to be zero

## 5. Spin 9/2

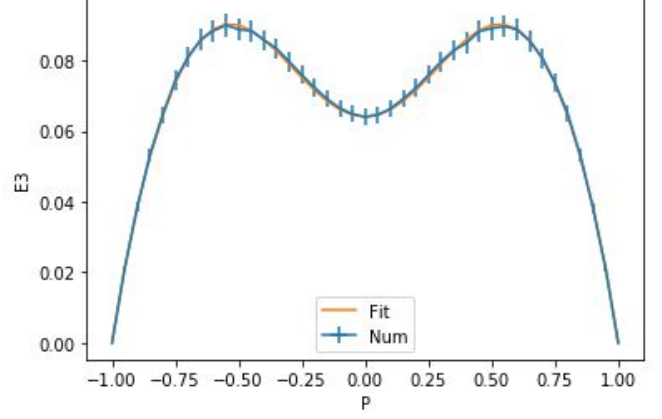


FIG. 21. Integral  $E_3$  as a function of the polarization for the case  $s = 9/2$ . The error-bars are represented, however in some points they are smaller than the width of the line. The fitting is also represented but it is behind the blue line.

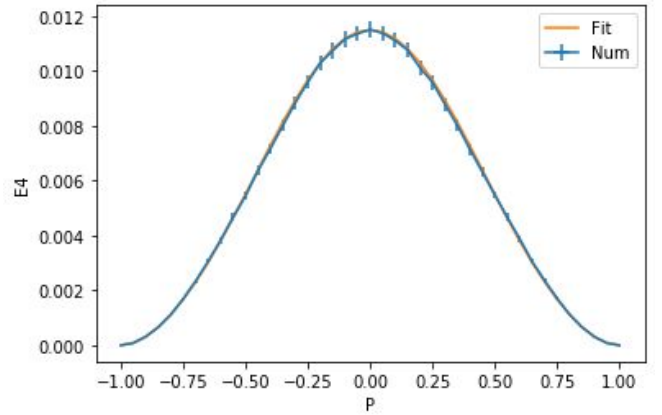


FIG. 22. Integral  $E_4$  as a function of the polarization for the case  $s = 9/2$ . The error-bars are represented, however in some points they are smaller than the width of the line. The fitting is also represented but it is behind the blue line.

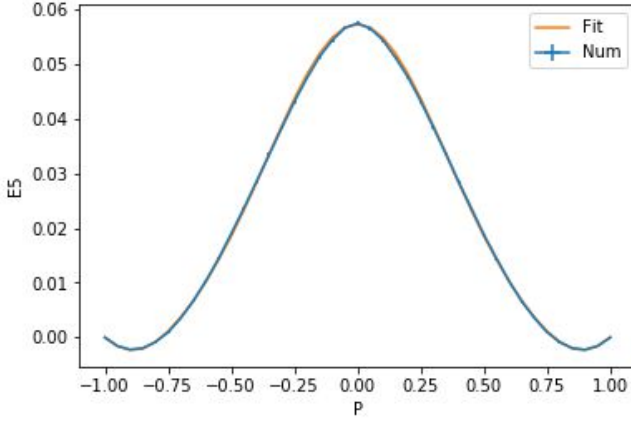


FIG. 23. Integral  $E_5$  as a function of the polarization for the case  $s = 9/2$ . The error-bars are represented, however in some points they are smaller than the width of the line. The fitting is also represented but it is behind the blue line.

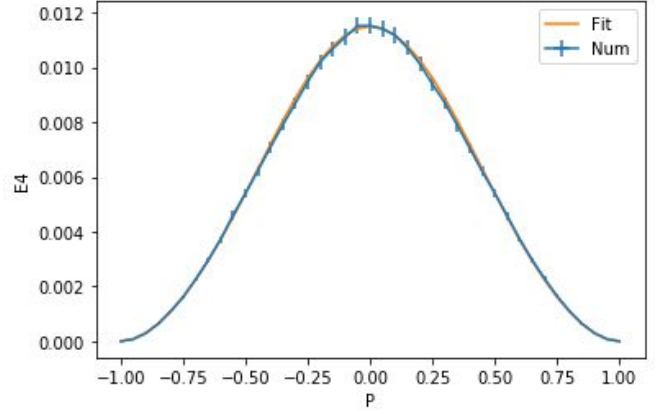


FIG. 25. Integral  $E_4$  as a function of the polarization for the case  $s = 11/2$ . The error-bars are represented, however in some points they are smaller than the width of the line. The fitting is also represented but it is behind the blue line.

	$b_1$	$b_2$	$b_3$	$b_4$	$\chi_{red}^2$
$E_3$	$4.22 \pm 0.04$	$-3.39 \pm 0.15$	$1.83 \pm 0.13$		0.04
$E_4$	$-1.731 \pm 0.018$	$1.28 \pm 0.05$	$-0.55 \pm 0.04$		0.19
$E_5$	$-3.32 \pm 0.04$	$5.6 \pm 0.2$	$-6.5 \pm 0.5$	$2.9 \pm 0.3$	1.02

TABLE VI. Parameters of the fit with their uncertainties, and the reduced chi square associated with each fitting for the case  $s = 9/2$ . The blank spaces can be considered to be zero

## 6. Spin 11/2

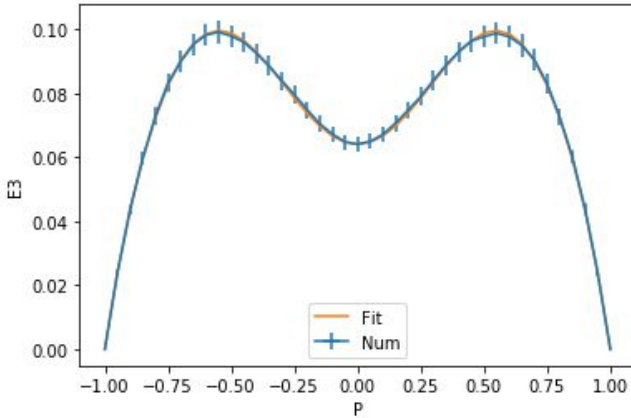


FIG. 24. Integral  $E_3$  as a function of the polarization for the case  $s = 11/2$ . The error-bars are represented, however in some points they are smaller than the width of the line. The fitting is also represented but it is behind the blue line.

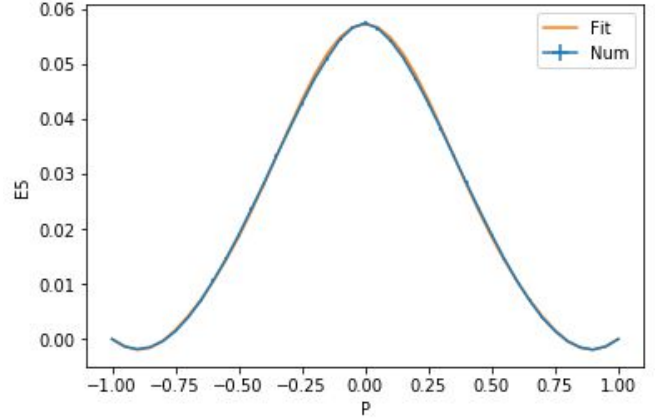


FIG. 26. Integral  $E_5$  as a function of the polarization for the case  $s = 11/2$ . The error-bars are represented, however in some points they are smaller than the width of the line. The fitting is also represented but it is behind the blue line.

	$b_1$	$b_2$	$b_3$	$b_4$	$\chi_{red}^2$
$E_3$	$5.19 \pm 0.04$	$-4.49 \pm 0.17$	$2.49 \pm 0.15$		0.04
$E_4$	$-1.81 \pm 0.02$	$1.42 \pm 0.06$	$-0.62 \pm 0.04$		0.24
$E_5$	$-3.42 \pm 0.05$	$6.2 \pm 0.3$	$-7.3 \pm 0.5$	$3.3 \pm 0.3$	1.77

TABLE VII. Parameters of the fit with their uncertainties, and the reduced chi square associated with each fitting for the case  $s = 11/2$ . The blank spaces can be considered to be zero

## 7. Spin 13/2

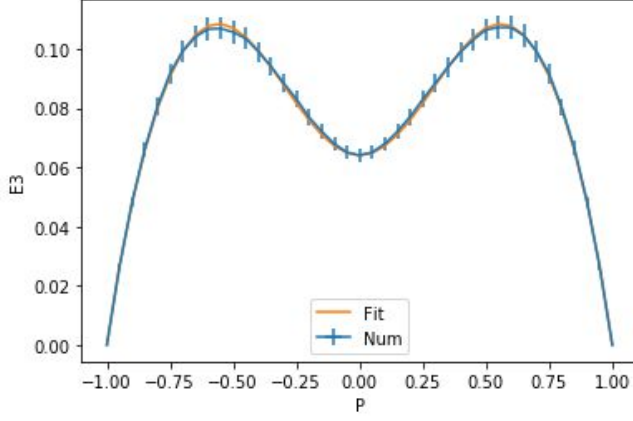


FIG. 27. Integral  $E_3$  as a function of the polarization for the case  $s = 13/2$ . The error-bars are represented, however in some points they are smaller than the width of the line. The fitting is also represented but it is behind the blue line.

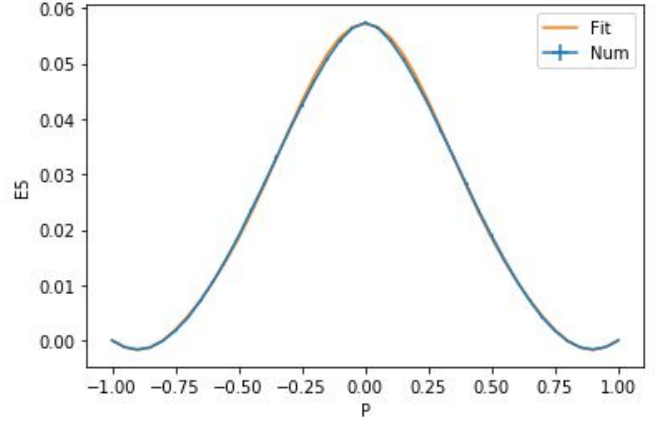


FIG. 29. Integral  $E_5$  as a function of the polarization for the case  $s = 13/2$ . The error-bars are represented, however in some points they are smaller than the width of the line. The fitting is also represented but it is behind the blue line.

	$b_1$	$b_2$	$b_3$	$b_4$	$\chi_{red}^2$
$E_3$	$6.08 \pm 0.06$	$-5.4 \pm 0.2$	$3.0 \pm 0.2$		0.07
$E_4$	$-1.90 \pm 0.02$	$1.62 \pm 0.06$	$-0.73 \pm 0.04$		0.25
$E_5$	$-3.52 \pm 0.05$	$6.7 \pm 0.3$	$-8.1 \pm 0.6$	$3.7 \pm 0.4$	2.70

TABLE VIII. Parameters of the fit with their uncertainties, and the reduced chi square associated with each fitting for the case  $s = 13/2$ . The blank spaces can be considered to be zero

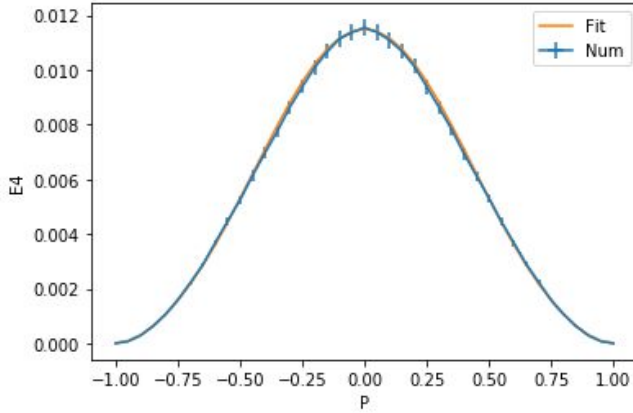


FIG. 28. Integral  $E_4$  as a function of the polarization for the case  $s = 13/2$ . The error-bars are represented, however in some points they are smaller than the width of the line. The fitting is also represented but it is behind the blue line.

## 8. Spin 15/2

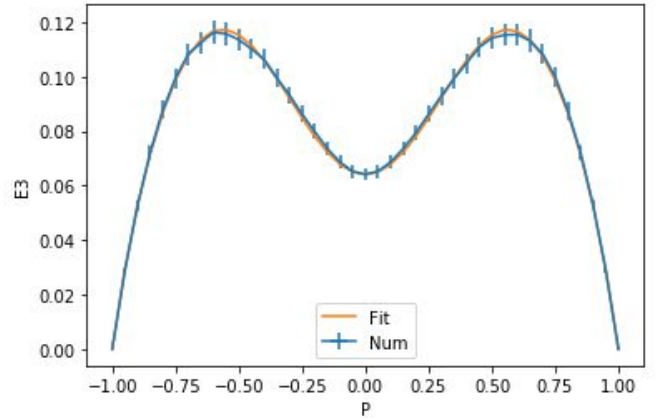


FIG. 30. Integral  $E_3$  as a function of the polarization for the case  $s = 15/2$ . The error-bars are represented, however in some points they are smaller than the width of the line. The fitting is also represented but it is behind the blue line.

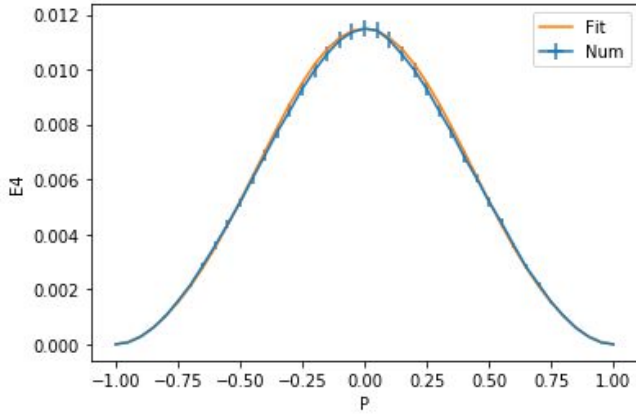


FIG. 31. Integral  $E_4$  as a function of the polarization for the case  $s = 15/2$ . The error-bars are represented, however in some points they are smaller than the width of the line. The fitting is also represented but it is behind the blue line.

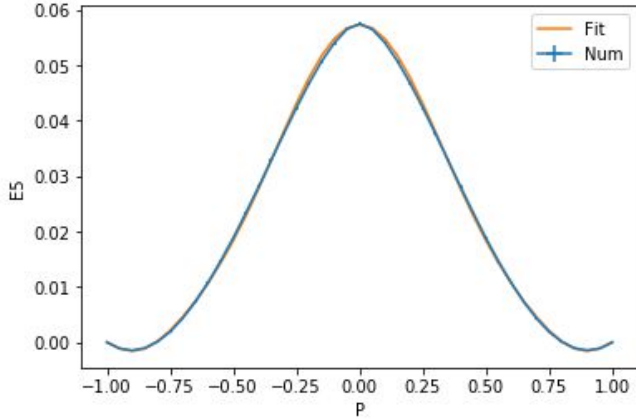


FIG. 32. Integral  $E_5$  as a function of the polarization for the case  $s = 15/2$ . The error-bars are represented, however in some points they are smaller than the width of the line. The fitting is also represented but it is behind the blue line.

	$b_1$	$b_2$	$b_3$	$b_4$	$\chi^2_{red}$
$E_3$	$7.00 \pm 0.07$	$-6.5 \pm 0.3$	$3.6 \pm 0.3$		0.10
$E_4$	$-1.96 \pm 0.03$	$1.71 \pm 0.07$	$-0.76 \pm 0.05$		0.44
$E_5$	$-3.59 \pm 0.06$	$7.1 \pm 0.4$	$-8.5 \pm 0.7$	$3.9 \pm 0.4$	3.82

TABLE IX. Parameters of the fit with their uncertainties, and the reduced chi square associated with each fitting for the case  $s = 15/2$ . The blank spaces can be considered to be zero

<sup>1</sup>C. Pfleiderer, S. Julian, and G. Lonzarich, “Non-fermi-liquid nature of the normal state of itinerant-electron ferromagnets,” *Nature* **414**, 427–430 (2001).

<sup>2</sup>M. Leduc, “Spin polarized helium-3, a playground in many domains of physics,” *Journal de Physique Colloques* **51**, C6–317–C6–331 (1990).

<sup>3</sup>Y. Ji, G. L. Schumacher, G. G. T. Assumpção, J. Chen, J. Mäkinen, F. J. Vivanco, and N. Navon, “On the stability of the repulsive fermi gas with contact interactions,” (2022).

<sup>4</sup>G. Valtolina, F. Scazza, A. Amico, A. Burchianti, A. Recati, T. Enss, and M. Inguscio, “Exploring the ferromagnetic behaviour of a repulsive fermi gas through spin dynamics,” *Nat. Phys.* **13**, 704 (2017).

<sup>5</sup>G. J. Conduit, A. G. Green, and B. D. Simons, “Inhomogeneous phase formation on the border of itinerant ferromagnetism,” *Phys. Rev. Lett.* **103**, 207201 (2009).

<sup>6</sup>S. Pilati, G. Bertaina, S. Giorgini, and M. Troyer, “Itinerant ferromagnetism of a repulsive atomic fermi gas: A quantum monte carlo study,” *Phys. Rev. Lett.* **105**, 030405 (2010).

<sup>7</sup>S.-Y. Chang, M. Randeria, and N. Trivedi, “Ferromagnetism in the upper branch of the feshbach resonance and the hard-sphere fermi gas,” *Proc. Natl. Acad. Sci. USA* **108**, 51 (2011).

<sup>8</sup>G. J. Conduit and B. D. Simons, “Itinerant ferromagnetism in an atomic fermi gas: Influence of population imbalance,” *Phys. Rev. A* **79**, 053606 (2009).

<sup>9</sup>P. Massignan, Z. Yu, and G. M. Bruun, “Itinerant ferromagnetism in a polarized two-component fermi gas,” *Phys. Rev. Lett.* **110**, 230401 (2013).

<sup>10</sup>X. Cui and H. Zhai, “Stability of a fully magnetized ferromagnetic state in repulsively interacting ultracold fermi gases,” *Phys. Rev. A* **81**, 041602 (2010).

<sup>11</sup>F. Arias de Saavedra, F. Mazzanti, J. Boronat, and A. Polls, “Ferromagnetic transition of a two-component fermi gas of hard spheres,” *Phys. Rev. A* **85**, 033615 (2012).

<sup>12</sup>S. Pilati, G. Orso, and G. Bertaina, “Quantum monte carlo simulations of two-dimensional repulsive fermi gases with population imbalance,” *Phys. Rev. A* **103**, 063314 (2021).

<sup>13</sup>G. Pagano, M. Mancini, G. Cappellini, P. Lombardi, F. Schäfer, H. Hu, X. J. Liu, J. Catani, C. Sias, M. Inguscio, and L. Fallani, “A one-dimensional liquid of fermions with tunable spin,” *Nat. Phys.* **10**, 198 (2014).

<sup>14</sup>A. Goban, R. B. Hutson, G. E. Marti, S. L. Campbell, M. A. Perlin, P. S. Julienne, J. P. D’Incao, A. M. Rey, and J. Ye, “Emergence of multi-body interactions in a fermionic lattice clock,” *Nature (London)* **563**, 369 (2018).

<sup>15</sup>E. Stoner, “Atomic moments in ferromagnetic metals and alloys with non-ferromagnetic elements,” *The London, Edinburgh, and Dublin Philosophical Magazine and Journal of Science* **15**, 1018–1034 ((1933)).

<sup>16</sup>K. Huang and C. N. Yang, “Quantum-mechanical many-body problem with hard-sphere interaction,” *Phys. Rev.* **105**, 767 ((1957)).

<sup>17</sup>T. D. Lee and C. N. Yang, “Many-body problem in quantum mechanics and quantum statistical mechanics,” *Phys. Rev.* **105**, 1119 ((1957)).

<sup>18</sup>V. M. Galitskii, “The energy spectrum of a non-ideal fermi gas,” *Journal of Experimental and Theoretical Physics* **7**, 104 ((1958)).

<sup>19</sup>I. M. K. A. A. Abrikosov, “Concerning a model for a non-ideal fermi gas,” *Journal of Experimental and Theoretical Physics* **6**, 888 (1958).

<sup>20</sup>J. Pera, J. Casulleras, and J. Boronat, “Itinerant ferromagnetism in dilute  $su(n)$  fermi gases,” (2022).

<sup>21</sup>S. Kanno, “Criterion for the ferromagnetism of hard sphere fermi liquid. ii,” *Prog. Theor. Phys.* **44**, 813 (1970).

<sup>22</sup>R. F. Bishop, “Ground-state energy of a dilute fermi gas,” *Annals of Physics* **77**, 106–138 (1973).

<sup>23</sup>P. Chankowski and J. Wojtkiewicz, “Ground-state energy of the polarized dilute gas of interacting spin- $\frac{1}{2}$  fermions,” *Phys. Rev. B* **104**, 144425 (2021).

<sup>24</sup>L. He and X.-G. Huang, “Nonperturbative effects on the ferromagnetic transition in repulsive fermi gases,” *Phys. Rev. A* **85**, 043624 (2012).

<sup>25</sup>G. A. Baker-Jr., “Study of the perturbation series for the ground state of a many-fermion system,” *Phys. Rev.* **140B**, 9 ((1965)).

<sup>26</sup>V. N. Efimov and M. Y. Amus’ya, “Ground state of a rarefied fermi gas of rigid spheres,” *Journal of Experimental and Theoretical Physics* **20**, 338 (1965).

<sup>27</sup>V. N. Efimov, “A rarefied fermi gas and the two-body scattering problem,” *Journal of Experimental and Theoretical Physics* **22**, 135 (1966).